Biochimica et Biophysica Acta, 936 (1988) 236–248
Elsevier

BBA 42886

Electron-spin polarization in the donor triplet state of bacterial photosynthetic reaction centers. I. Microsecond time-resolved EPR of *Rhodopseudomonas viridis* reaction centers

Fred G.H. van Wijk * and Tjeerd J. Schaafsma

Department of Molecular Physics, Agricultural University, Wageningen (The Netherlands)

(Received 5 August 1988)

Key words: Reaction center; Triplet state; Electron spin polarization; Decay rate; Relaxation mechanism; (*Rps. viridis*)

The EPR transients in the three canonical transitions of the $\Delta m = \pm 1$ triplet spectrum of *Rhodopseudomonas viridis* RC's have been measured following a 10 ns laser-flash. At microsecond time-resolution, the initial amplitude of these transitions at 100 K is inverted for the Y peaks, zero for the Z peaks, and not affected (thus firmly emissively polarized) for the X peaks as compared to the initial amplitudes at $T < 10$ K. This demonstrates that temperature-dependent processes in the precursor state P^F affecting the populating rates of the sublevels of the primary donor triplet state (P^R) are responsible for the temperature-dependent changes of the electron spin polarization (ESP) pattern. The P^R decay rate constants after correcting for spin lattice relaxation (SLR) contributions for all three canonical axes do not change with temperature from 4 K to 100 K. The observed increase in decay rate constants is explained invoking a relaxation mechanism probably operating via P^F, or a relaxed form of it. At $T > 40$ K the SLR process does not affect the observed decay rate constants anymore. It is proposed that above 40 K the initial ESP (i.e., at approx. 1 μs after the laser flash) and the steady-state ESP approach each other, reducing the effect of the relaxation process. Creation of P^F from P^R, which is populated by T–T energy transfer from the antenna triplet, is proposed as a mechanism explaining the observed spin relaxation and polarization of P^R.

Introduction

The primary donor triplet state (P^R) in photosynthetic reaction centers (RC's) is exclusively generated via the charge-separated state P^+I^-, where P^+ is the oxidised primary donor and I^- the reduced intermediary electron acceptor. The electron spin polarization (ESP) of P^R in high magnetic fields is determined by the spin dynamics

* Present address: AKZO Research, Corporate Research Dept. (CRL), P.O. Box 60, 6800 AB Arnhem, The Netherlands.

Abbreviation: RC, reaction center; SLR, spin lattice relaxation.

Correspondence: T.J. Schaafsma, Department of Molecular Physics, Wageningen Agricultural University, De Dreijen 11, 6703 BC Wageningen, The Netherlands.

within P^+I^- [1–8]. Actually, for reduced RC's, P^+I^- forms part of the state $P^+I^-Q_A^-Fe^{2+}$, in the following denoted P^F, where Q_A^- represents the primary electron acceptor and Fe^{2+} has $S = 2$.

When the forward electron-transfer reaction is blocked by removal or reduction of Q_A, the lifetime of P^F increases from approx. 200 ps [9–11] to 10–20 ns [8,11,22], thereby allowing rephasing of the electron spins in P^F. At sufficiently low temperatures ($T < 20$ K) [12], and in high magnetic fields, P^F recombines exclusively into the $m_S = 0$ sublevel of P^R. As a result the $\Delta m = \pm 1$ triplet EPR spectrum of P^R under continuous illumination exhibits an AEEAAE (A = enhanced absorption, E = emission) steady-state electron spin polarization (SSESP) pattern [1–3]. This pattern is characteristic for photosynthetic RC's [1,13–15] which are photochemically active at the donorside, generating P^R via the radical pair mechanism [2–8].

Recently, we observed however that the AEEAAE ESP pattern reversibly converts into AEAEAE at $T \approx 20$ K for reduced RC's, isolated from *Rhodopseudomonas viridis* [16,17] (See Fig. 1). A similar, but less pronounced temperature-dependent change was found for chromatophores of *Chromatium vinosum* [17] and RC's from *Rhodobacter sphaeroides* R-26 [18]. The extent of this change correlates with the magnitude of the magnetic interaction between I^- and Q_A^-. In agreement with this, reduction of Q_A^- to the diamagnetic Q_A^{2-} anion eliminates the polarization inversion [19]. Finally, when the magnetic interaction between Fe^{2+} and Q_A^- is reduced or destroyed (e.g., by SDS-treatment, or removal of Fe^{2+} and/or Q_A) the AEEAAE ESP pattern is preserved at all temperatures (8–120 K).

From these results it was concluded that the observed temperature dependence of the ESP in P^R is due to the presence of Fe^{2+} as a strong source for spin-relaxation, transmitted to I^- via Q_A^- in P^F. Previously, several authors have realized that the third electron spin on Q_A^- had to be included for a proper description of the magnetic interactions in P^F [23,24].

In order to investigate the effect of a temperature dependent spin lattice relaxation (SLR) of this third spin in P^F on the electron-hole recombination to the $|+1>$, $|0>$, and $|-1>$ sublevels

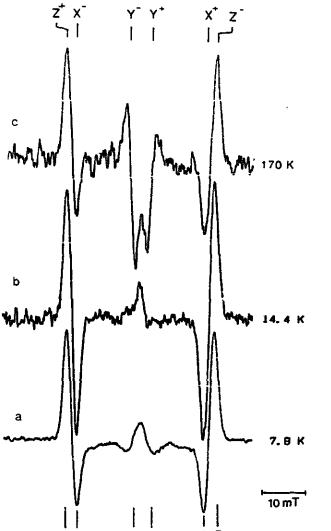

Fig. 1. Light-minus-dark steady-state $\Delta m = \pm 1$ triplet EPR spectra of P^R in *Rps. viridis* RC's at various temperatures 'A' denotes enhanced and 'E' emissive absorptive transition. X, Y, and Z mark the canonical field positions, the superscripts '+' and '−' indicate whether a $|0\rangle \leftrightarrow |+1>$ or a $|0> \leftrightarrow |-1\rangle$ transition is observed. Experimental conditions: A_{830} (RC's) = 30. All samples contained 1 mM sodium ascorbate, were threefold diluted in ethylene glycol and frozen in the dark. Light-modulation frequency: 400 Hz; light source: 150 W Xe-lamp, filtered through 6 cm water. Microwave power: 500 μW in a and b, 1 mW in c. Magnetic-field modulation amplitude: 1.6 mT at 100 kHz. Center field position 326 mT.

of P^R, we studied the response of the $\Delta m = \pm 1$ triplet EPR transitions of P^R on a microsecond timescale, following an approx. 10 ns optical excitation pulse.

The initial ESP pattern (denoted IESP), observed within approx. 1 μs after generating P^R, reflects the relative populating rates (i.e., relative quantum yields of formation) of the P^R sublevels from P^F, and thus yields more direct information

on the temperature dependence of the spin transitions within P^F than steady state measurements on P^R. Note that on a microsecond timescale, P^F has completely decayed to P^R, but the population of P^R has not noticeably changed.

Time-resolved EPR also provides information on the SLR processes within P^R and their temperature-dependence [20,21]. Optical studies have shown that the decay rate constants of P^R are temperature-independent in the range 0–150 K [25], but increase at $T > 150$ K.

The rate of the back electron-transfer reaction $P^+Q_A^-$ to P^*Q_A was studied by several groups in RC's of *Rb. sphaeroides* R-26 [26,27]. These studies suggest that, at least at higher temperatures, a back reaction from P^R into P^F (or a relaxed state of P^F) is involved, increasing the rate of the $P^+Q_A^-$ recombination process, and thus also the observed P^R decay rate constants. Studies on the effect of a magnetic field on the triplet state lifetime led to the same conclusion [23].

This paper (part I) treats the effects of temperature-dependent relaxation within P^F and P^R of *Rps. viridis* on the populating and depopulating processes of the P^R sublevels from an experimental point of view. The subsequent paper (part II [42]) presents a theoretical model to explain the observed change in the ESP pattern of P^R, involving the g-value anisotropy of the $Fe^{2+}Q_A^-$ complex in photosynthetic bacteria.

Materials and Methods

Cells of *Rps. viridis* were grown anaerobically [28] (Budil, D.E., personal communication). RC's were isolated as described in Ref. 29, with a slight modification as described in Ref. 30. LDAO was used as a detergent.

EPR samples were prepared as described in Refs. 15, 29, using sodium ascorbate to assure reduction of the cytochromes and the primary donor, followed by rapid freezing in the dark. Photoreduction generated the PIQ_A^- state in the RC's.

The time-resolved EPR measurements were carried out using a novel method as described in Ref. 31. Briefly, the standard phase-sensitive detector of the X-band EPR spectrometer (Varian E6) was by-passed, and replaced by a modified broad-band phase-sensitive detector (B-PSD) (Brookdeal) with sub-microsecond time-resolution. A high-pass (filter at the input of the B-PSD was employed (−3 dB point at 100 kHz), replacing the tuned amplifier which is a standard component of lock-in detectors. The low-pass filter at the output of the B-PSD was removed. The magnetic field modulation frequency was 200 kHz, which slightly improves the fidelity of the obtained transient as compared to the more usual 100 kHz modulation frequency. EPR signals were averaged randomly with respect to the modulation frequency, averaging out the rectified sine waves from the output of the B-PSD. A LeCroy 3500 signal analyzer was used to digitize and average the EPR transient signals, optically triggered by the exciting laser flash. The overall time-resolution was 750 ± 150 ns, with a d.c. to 1 MHz frequency response from d.c. to a.c. in MHz. Typically, 5000 transients were averaged in each run to obtain a satisfactory S/N ratio.

Even for the first derivative EPR spectra the X and Y transients may contain residual contributions from other than the canonical ones. In order to estimate these contributions, transients were recorded at magnetic-field positions halfway between Z^+ and X^-. Under the above-mentioned experimental conditions no transient could be detected. Therefore, no corrections were made for the contributions of non-canonical orientations to the canonical transients.

Excitation was from a Q-switched Nd:YAG pulse laser (JK HY-200), frequency doubled (532 nm, 30 mJ/pulse) pumping a home built high-gain broadband tunable pulsed dye laser [32]. A 1:1 mixture of Rhodamine 6G and Rhodamine 101 in methanol was used to obtain laser flashes with $\lambda = 612$ nm (3 nm FWHM), 1–2 mJ/pulse and a pulse duration of 10 ns. Excitation repetition rate was 21 Hz, running freely from the EPR magnetic field modulation frequency (200 kHz, see above). The laser beam entered the EPR cavity (Varian, rectangular E-231 operating in TE_{102} mode) through a light tube in the front of the cavity, taken from an optical transmission cavity.

The intense laser flash generates a spurious transient in the EPR cavity, orginating from heating of the side walls by scattered light. This artefact is partly subtracted by the magnetic-field modula-

tion method, since its amplitude does not depend on the magnetic field position, whereas the true EPR signal from P^R does. Part of the signal remains, but can be further reduced by the averaging process. The phase of the artefact (present in the first few μs after the laser flash) is more or less random, whereas the phase of the EPR signal is always the same. Therefore, the laser flash artefact is substantially reduced with respect to the amplitude of the EPR signal by the averaging process. For those transients where the first few microseconds are less important (i.e., for transients with relatively long decay times), the signal at the input of the B-PSD was blocked during the first 5 μs by a FET gate 4066 driven by the laser excitation. In more critical experiments the interior of the cavity was covered by carbonblack paper (except the back and front side), reducing the light-induced spurious transient by a factor 5–10, but reducing the loaded Q-factor of the cavity. This results in a net improvement of the S/N ratio of a factor 2–5. Further details are given in Ref. 30.

Exponential functions were fitted using the method described by McLachlan [34], employing a Rainbow 100 microcomputer interfaced to the LeCroy 3500 signal analyzer. For transients consisting of two exponentials this method was extended by an iterative subtraction of the calculated exponential from the experimental transient to calculate the residual exponential. Whether a given curve is best fit by a single or a double exponential, was decided upon by visual inspection of the residual plots.

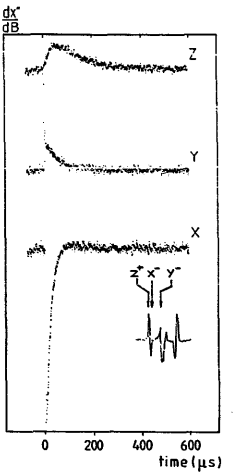

Fig. 2. EPR transients from P^R in RC's from *Rps. viridis* detected at 100 K. The transients are recorded at the peak positions of the steady-state $\Delta m = \pm 1$ triplet EPR spectrum as indicated by the arrows in the inset. Experimental conditions: microwave power: 200 μW, magnetic field modulation frequency: 200 kHz, modulation amplitude: 2.5 mT, excitation: 21 Hz, 12 ns pulse duration, 2 mJ/pulse, excitation wavelength: 612 nm. Sample: $A_{830} = 40$. 100 μl RC's in 200 μl ethyleneglycol. Photoreduction by 1 mM sodium ascorbate. Transient recorder: pretrigger period of 1/8 sweep; start of transient at $t = 0$.

Results

Fig. 2 shows the EPR transients at 100 K recorded in the peaks of the first derivatives $\Delta m = \pm 1$ triplet spectrum as indicated by arrows in the inset. The spectra were recorded using the pretrigger facility of the signal analyzer. Therefore the laser flash arrives at 1/8th of the horizontal (time) axis. Note the entirely different signal amplitude at $t = 0$ μs of the X, Y and Z transients.

In order to investigate whether the observed changes in ESP pattern originate in P^F, the temperature dependence of the decay rates from the sublevels of P^F to those of P^R should be determined. These are approx. 10^8 s^{-1} [11], and are too fast to be recorded by EPR spectrometers. However, the IESP pattern of P^R, corresponding to the ESP pattern observed in the first microsecond of the EPR transients in Fig. 2, contains the same information, since SLR or decay of the P^R spin levels does not contribute to the transient amplitudes at a microsecond timescale (see below). The initial spectrum exhibits an –EAEA– ESP pattern, where '–' denotes zero amplitude for the Z transitions. The transients of the three corresponding high-field transitions are not shown in Fig. 2, since these are identical to those which are shown. The time-integrated ESP pattern, corresponding to spectra as observed under continuous

TABLE I

(A) DECAY RATE CONSTANTS k_0 AND $k_{\pm 1}$ OF P^R AT $T \leq 8$ K. (B) DECAY RATE CONSTANTS k_1, k_2 AND RELATIVE POPULATING RATES p_1, p_2 DESCRIBING THE TRANSIENTS AT $T = 40$–100 K FOR THE X, Y AND Z TRANSITIONS.

A: $T \leq 8$ K (see Ref. 39)

Transition	$k_{\pm 1}$ (10^3 s^{-1})	k_0 (10^3 s^{-1})
X	9 ± 0.5	14 ± 1
Y	8 ± 0.5	16 ± 1
Z	15 ± 1	2.4 ± 0.1
	$\langle k \rangle$ [a] $= (11 \pm 1) \cdot 10^3$ s^{-1}	

[a] Calculated from $\langle k \rangle = \frac{1}{3}(k_0 + 2k_{\pm 1})$.

B: $T = 40$–100 K

Transition	k_1 (10^3 s^{-1})	p_1 (%)	k_2 (10^3 s^{-1})	p_2 (%)
X	55 ± 5	95 ± 5	9 ± 2	5 ± 5
Y	50 ± 5	10 ± 20	14 ± 6	90 ± 20
Z	50 ± 10	50 ± 10	11 ± 2	50 ± 10

illumination, is AEAEAE, in accordance with previous results [16,17].

The transients in Fig. 2 at 100 K exhibit several differences with those obtained at 8 K (not shown).

(i) At 8 K the IESP pattern is AEEAAE, whereas at 100 K –EAEA– is found;

(ii) the decay rate constants at 100 K obtained by a two-exponential fit of the EPR transients of the X and Z peak have increased with regard to those at 8 K, but the decay rate constant of the Y transition has decreased (see Table I);

(iii) at $T \leq 8$ K all transients show single exponential decay at a microwave power low enough to make sure that the EPR signal is not noticeable influenced [21]. The observed decay rate constants are in agreement with literature [39] and represent the experimental value of k_0 for the X, Y and Z transients (see Table I), since T_0 is predominantly populated at this temperature. At 100 K, however, four out of six transients follow a two-exponential decay even at very low microwave power. The Y^+ and Y^- transients follow a single exponential decay and represent predominant decay from the $T^{\pm}$ sublevels of P^R according to this sign.

A temperature study of the steady-state EPR spectra showed the disappearance of the Y peaks in the temperature range 16–22 K [17]. Fig. 3 shows the transients detected at 17 and 40 K of the two EPR transitions which change most strongly with temperature: Y and Z (the relative amplitudes of the EPR transients of the X-transitions hardly change with temperature). As is evident from this figure, the IESP of the Z peaks is absorptive for both temperatures. The same result is observed for the IESP of the Y transitions. Keeping in mind that the Y transients of Fig. 2 are monitored at the center positions between both Y peaks, a positive Y signal implies an emissive IESP. For more details, see Fig. 1. However, time-integration of the Y transient yields about zero amplitude at 17 K, and a net absorptive signal at 40 K. Time-integration of the Z transient yields a net absorptive signal for both temperatures. These observations are in agreement with the SSESP pattern at the same temperatures [17].

Fig. 4 shows the temperature dependence of the ratio of amplitudes of the EPR transients in the first microseconds of the exponential components. This ratio equals that of the relative populating rates p_i ($i = \pm 1, 0$) of the sublevels $|\pm 1>$ and $|0>$ of P^R. By definition $\Sigma p_i = 1$. This ratio represents the relative populating rate from P^F to the $T_{\pm}$ and T_0 sublevels of P^R. Ratios p_1/p_0 larger than unity represent preferential populating of the $T_{\pm}$ sublevels. The spread in the measured p_1/p_0 ratio is rather large, since the flash artefact affects the initial amplitudes of the exponentials. In addition, for small contributions of one of the exponential components, the fit becomes relatively less accurate with respect to the initial amplitude. For the static magnetic field $B_0 // Y$ two of the three transients observed at approx. 100 K (see Fig. 4b) follow a single exponent, leading to $p_1/p_0 \rightarrow \infty$ due to the very low value of p_0. Considering the S/N ratio, finite p_1/p_0 ratios are not excluded.

To investigate whether the change of the observed decay rate constants is due to an increase of the SLR rate constants w within P^R, the experimental data were fitted with various intramolecu-

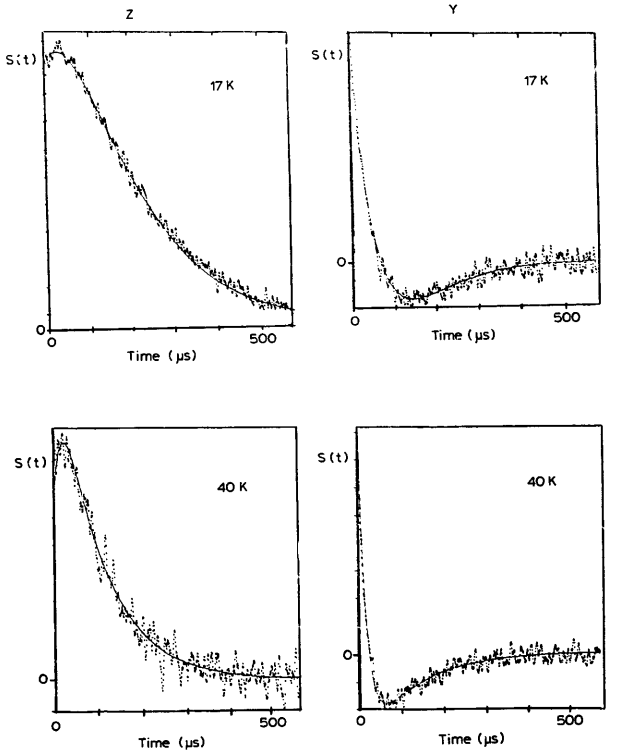

Fig. 3. Z and Y EPR transients from P^R in RC's from *Rps. viridis* detected at 17 K and 40 K. Conditions were identical to those given at Fig. 2, but no pretrigger period was used. Solid lines represent fitted curves.

lar relaxation models:

(i) using three different rate constants for relaxation between each of the three sublevels;

(ii) equal rate constants for relaxation between each of the sublevels; and

(iii) the model given in Fig. 5, i.e., equal rate constants for relaxation between only two of these sublevels.

Only the model given in Fig. 5 yielded results in accordance with Fig. 6a–c. In these calculations the values of the decay rate constants k_0 and k_1 of the T_0 and $T_{\pm 1}$ sublevels at 4 K were assumed to be independent of temperature in the experimental range $T = 4$–120 K. The increase in observed decay is then entirely due to the SLR process.

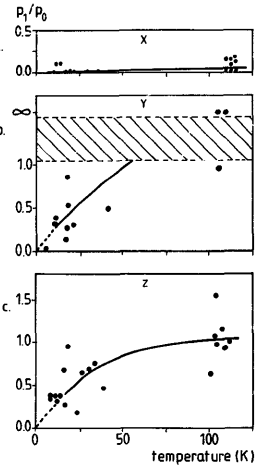

Fig. 4. Ratio of amplitudes (i.e., the relative populating rates) associated with the exponential decay constants making up the experimental transients. p_1 refers to the populating channel of the $T_{\pm}$ spin levels of P^R, p_0 refers to the populating channel of the T_0 spin level of P^R. (a) transients detected in the X transitions of the $\Delta m = \pm 1$ triplet EPR spectrum; (b) idem in the Y transitions. For zero population of the T_0 spin level the p_1/p_0 ratio becomes infinite. Due to their limited accuracy the experimental points at approx. 100 K fall in the hatched region between 1 and ∞; (c) transients detected in the Z transitions.

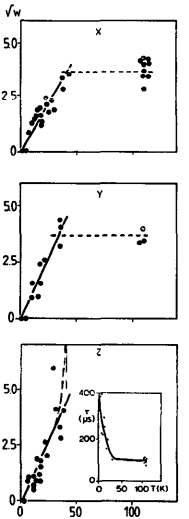

Fig. 6. The relation between $w^{1/2}$, where w denotes the spin-lattice relaxation rate (expressed in 10^3 s^{-1}) as measured at the canonical field positions ($B_0//X$, Y and Z) and temperature. Dots represent experimental values for w (see Appendix A). The solid line represents a fit, using the empirical relation $w = aT^2$. For $B//X$ $a = 0.010 \pm 0.001$, for $B//Y$ and $B//Z$ $a = 0.012 \pm 0.001$ was used to fit the experimental data. Inset: temperature dependence of the decay time τ present in the transients.

Due to the fact that in high field the decay rate constants for T_+ and T_- are identical, the transient EPR signal of P^R contains a maximum of two exponential decay rate constants [34]. One of these corresponds to the largest of the two decay rate in the low-temperature limit, and continues to increase with increasing SLR. The other approaches the mean value $\langle k \rangle = \frac{1}{3}(k_0 + 2\,k_1)$ with increasing SLR, and extrapolates to the smallest of the two decay rate constants in the low-temperature limit. The mean decay rate constant would be observed in full thermal equilibrium, i.e., when the relaxation process is much faster than the

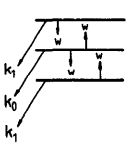

Fig. 5. Kinetic scheme for P^R. k_1 and k_0 denote the low-temperature ($T \to 0$) decay rate constants from the $T_{\pm}$ and T_0 P^R sublevels to the singlet ground state of P-960. w denotes the relaxation rate constant.

decay rates, resulting in a 1 : 1 : 1 spin distribution over T_+, T_0 and T_-. For the values of k_0 and k_1 at 4 K, see Table I.

In the intermediate case, when the relaxation rate is of the order of the decay rate, both exponential decay rate constants will be observed. The observed decay rate (k_0 for all transitions at $T \approx 5$ K, i.e., without SLR) increases with temperature, and the transients start to follow a two-exponential decay.

The exponential with the largest amplitude at $T < 10$ K of the two observed decay rate constants was used to calculate the magnitude of w presented in Fig. 6. In practice this exponential only contains k_0, since in the low temperature limit (when almost exclusive T_0 populating occurs) only k_0 is observed. The temperature dependence of w (see Appendix A) was fitted to the expression $w = aT^2 + b$ and for the X and Y transitions is expected to increase continuously with temperature, since $k_1 > k_0$. Fig. 6 shows the fit of the experimental results to this expression, leading to the remarkable result that above 35–40 K the observed decay rate constants do not further increase. For the Z transition the situation is only mathematically different: $k_0(Z)$ is smaller than $k_1(Z)$, thus the observed decay rate is expected to increase until it reaches the value $\langle k \rangle$ becoming independent of w at higher temperatures, as happens indeed at $T > 40$ K (see inset). The extraction of the experimentally observed SLR rate constant from the observed lifetimes (the experimental points in the inset of Fig. 6), yielded very large values of w at temperatures above 40 K. The method of extracting the value of w from the observed EPR decay rate constants is given in Appendix A.

The three parts of Fig. 6 all show that at a temperature of about 35 K the relative populations of the P^R sublevels become independent of temperature and thus independent of a further increase of w. Note, however, that this high-temperature equilibrium distribution over the sublevels of P^R does not correspond to a Boltzmann distribution, as is also evident from the steady-state ESP pattern at this temperature [17].

At 40–100 K the observed decay rate constants and their relative amplitudes in the transients are given in Table I.

Discussion

First we will discuss experimental results with respect to the fate of P^R in the first microsecond after generation of P^R. Since this period is short with respect to the lifetimes and SLR times of P^R, we observe the relative populating rates of the P^R spin levels. These rates are related to the spin dynamics of P^F, because any process affecting the probabilities to find a particular spin configuration within P^F must also result in a change of the relative populating rates of the sublevels of P^R, since $P^F \rightarrow P^R$ transitions are spin conserving. Although the reaction centers are excited by a coherent light source, the excitation at 600 nm is followed by radiationless decay to S_1, and subsequently to the radical pair. Spatial or temporal coherence between the radical-pair states of individual reaction centers therefore cannot occur. Microsecond transient EPR eliminates to a great extent complicating effects due to processes within P^R, such as decay from its sublevels and SLR, since these processes take place at a much longer time-scale.

In the second part of the discussion we will take a closer look at the time development (i.e., the decay) of the EPR transients of P^R at $t \gg 1$ μs, and the temperature dependence of spin-lattice relaxation within P^R contained in the observed decay rate constants. Temperature-dependent SLR within P^R alone cannot result in the observed change in the SSESP pattern of the $\Delta m_S = \pm 1$ EPR spectrum [16,17] (see Appendix B). However, as will be shown below, the temperature dependence of the SLR rate constants for P^R is unusual, and leads us to propose that P^F, or a relaxed form of it, is involved in this SLR process. This can lead to an enhancement of the electron spin polarization.

Decay from P^F

The Hamiltonian for P^F is given by (see also II):

$$\mathcal{H} = \mu_B \hbar^{-1} \sum_{i=1}^{3} g_i \mathbf{S}_i \cdot \mathbf{B}_0 - J_{23}(\tfrac{1}{2} + 2\mathbf{S}_2 \cdot \mathbf{S}_3) \qquad (1)$$

where 1, 2 and 3 denote the electronic spins on

P^+, I^- and Q_A^-, respectively; g_i is the g-value of electron spin i, μ_B denotes the Bohr magneton; B_0 is the external magnetic field of the EPR spectrometer; J_{23} denotes an exchange interaction – assumed to be isotropic – between spins 2 and 3.

The Hamiltonian (1) contains all strong magnetic interactions present in the RC of *Rps. viridis*, and is therefore expected to represent a good qualitative description of P^F.

In order to estimate the probability of finding a triplet state spin configuration (of spins 1 and 2) within P^F, the time dependence of the eigenfunctions of (1) must be found. It is straightforward to show that the probability of finding a triplet state spin configuration ϕ_i combined with a particular spin state S of spin 3 (e.g., $\phi_i = T_o(1,2)$; $s = \alpha(3)$) in P^F is given by:

$$|c_{\phi_i s}(t)|^2 = \left| \sum_{s',\alpha,\beta} \sum_{j=1}^{8} \langle Ss'|\Psi_j\rangle\langle\Psi_j|\phi_i s\rangle \exp\left\{-\frac{i}{\hbar}E_j t\right\} \right|^2 \tag{2}$$

where $|Ss'\rangle$ denotes the singlet spin function $|S\rangle$ of the spins 1 and 2, combined with spin 3 in spin state $|s'\rangle$. $|\Psi_j\rangle$ denotes the jth eigenfunction of Eqn. 1 with energy E_j.

The time evolution of $|c_{T_\pm}(t)|^2$ or $|c_{T_0}(t)|^2$ depends on ϕ_i. Using experimental values for J_{23} and Δg ($\Delta g \equiv g_2 - g_3$) [35], it is found that the frequency of the quantum beats for the amplitude of the T_+ and T_- sublevels is larger by a factor of approx. 5 with respect to the overall frequency of the $|T_0\rangle$ and $|S\rangle$ states in P^F. The maximum amplitude of the $T_\pm$ probability beats is, however, much smaller than for the singlet and T_0 probabilities as shown in Ref. 30.

These calcualtions also show that, at low temperature, when SLR of Fe^{2+} can be neglected, some mixing of $T_\pm$ with T_0 and the singlet state S occurs in P^F (in the presence of the spin on Q_A^-), due to the magnetic interaction between I^- and Q_A^-. Using experimental values for J_{23} and Δg and a lifetime of p^F of 15 ns, a few percent of $T_\pm$ is expected at low ($T \leqslant 5$ K) temperature. Thus, even at low temperature, the T_+ and T_- substates of P^R are populated, albeit not enough to affect the ESP pattern of the $\Delta m = \pm 1$ EPR triplet spectrum from P^R, in accordance with the experimentally observed AEEAAE pattern at $T < 10$ K [17]. Summarizing, the exclusive S–T_0 mixing, characteristic for the two-electron RP mechanism is replaced by a mechanism which may also generate T_+ and T_- spin states in P^R.

The transients in Fig. 2 provide evidence that the initial FSP of P^R results from the spin dynamics in the precursor state P^F of reduced RC's from *Rps. viridis*. Previously we suggested [16–19] that the SLR in paramagnetic Fe^{2+} is the source of the temperature dependence of the ESP pattern of the $\Delta m = \pm 1$ triplet EPR spectra of P^R. This relaxation is transmitted to the P^+I^- radical pair by the unpaired spin on the reduced primary acceptor (Q_A^-). Note that this relaxation process does not impose a Boltzmann equilibrium population distribution on the substates of P^F, since such a distribution, at 100 K, would have been monitored as almost zero signal intensity at $t \approx 10$ μs (i.e., in the first microsecond after generation of P^R). The transient of the Y transitions of P^R clearly shows an inverted population distribution

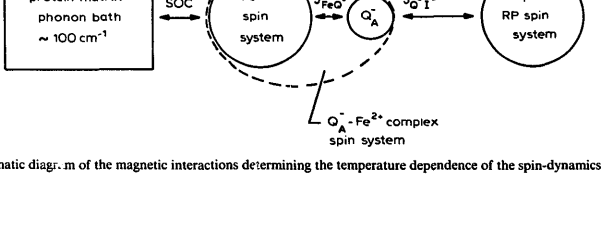

Fig. 7. Schematic diagram of the magnetic interactions determining the temperature dependence of the spin-dynamics within P^F.

with respect to the low-temperature distribution (mainly T_0 populated). Therefore, it must be concluded that, in the temperature region of the experiments (8 K $\leqslant T \leqslant$ 120 K), the spin dynamics at high magnetic field in the state P^F is affected by the relaxation processes of Fe^{2+}. The order of events is visualized in Fig. 7. The average lifetime of a particular spin state ($s' = \alpha$ or β) of the Q_A^- electron spin in the quinone-iron complex never becomes much shorter than the lifetime of P^F, otherwise a fully relaxed P^F state would have been monitored by the initial population distribution of P^R, nor much longer than the lifetime of P^F, otherwise no temperature effect at all would have been observed.

For the multi-level P^F system the quantitative effects of relaxation can only be calculated numerically (see part II: Ref. 42).

Decay from P^R

The kinetics of P^R show an unexpected temperature dependence.

(i) The SLR rate is found to be relatively slow in *Rhodopseudomonas viridis* as compared to, e.g., *Rhodobacter sphaeroides* [20,21]. In the latter $1/T_1$ is about 250 ms^{-1} at 100 K, whereas in *Rps. viridis* this rate is found to be approx. 10 ms^{-1} at the same temperature.

(ii) The temperature dependence of the relaxation rate reaches a plateau around 40 K.

(iii) The relaxation rate shows a quadratic dependence on temperature in the first 40 K.

The model we used to obtain rate equations to fit the experimental data is shown in Figs. 5 and 8. Both exponentials present in the transient yield a decay constant which does not vary in the temperature range 40–100 K. One of these exponentials has a rate constant close to the mean triplet decay rate $\langle k \rangle$. This indicates that the population distribution over the P^R sublevels does not change anymore during the observation time, i.e., typically during the average decay time $\langle k \rangle^{-1}$ of P^R. However, at this temperature the observed ESP pattern indicates a non-Boltzmann population distribution in P^R. We therefore conclude that relaxation does not take place within P^R, but in another state, connected to P^R. If the other state relaxes fully above 40 K, then no further effect is

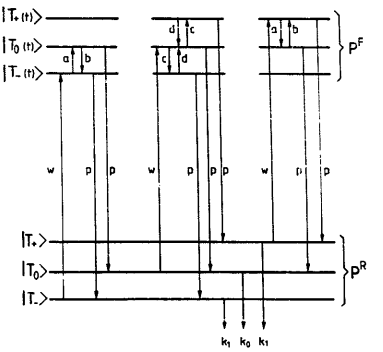

Fig. 8. Kinetic scheme to model the coherent and stochastic processes within P^F (rate constants a–d), and the transitions between P^F and P^R (rate constants p and w); k_1 and k_0 represent the decay rate constants of P^R at $T \to 0$. The time-dependent probabilities to find any spin configuration in P^F (T_+, T_- or T_0) depend on the spin configuration in which P^F is born. The three schemes of P^F represent the three different ways by which P^F can be generated from P^R. From left to right: generation in T_-, T_0 and T_+.

expected to the observable in P^R. However, the relaxation process in the other state apparently does not impose a Boltzmann distribution on P^R. This would be possible if spin scrambling occurs in the other state, which we shall call P^X. Repopulating P^R from P^X does not yield the original spin state.

What is the nature of P^X?

Recently, Woodbury et al. [26] proposed the existence of a second, more relaxed, RP state below the unrelaxed RP state P^F which we have so far discussed. Chidsey et al. [23] invoked back transitions from P^R into P^F to explain their optical, temperature dependent magnetic field effects in RC's from *Rb. sphaeroides*. Our results support the involvement of the charge separated state P^F (relaxed or not) at higher temperature in the kinetic pathway of P^R: since P^F does not consist of a pure triplet state, thermal repopulating P^F from P^R in a triplet spin configuration is followed by spin scrambling within P^F. Spin-rephasing within P^F is fast because the g-value differences between $g_{1,2}$

and g_3 are substantial, and quite different from the situation in the 'pure' radical pair. Once in P^F, the correlation of the spins may be lost due to the spin transitions caused by the Fe^{2+}. The recombination probabilities, regenerating P^R, are only determined by the magnetic interactions within P^F, i.e., a replay of the processes leading to the first populating process of P^R, yet different, since P^F is now born from a T_0 or a $T_\pm$ state in P^R, instead of from the singlet state P^*.

A kinetic scheme for the mechanism described above is given in Fig. 8, and is equivalent to the simplified model given in Fig. 5. It is evident from the observed relaxation rates (see Fig. 6), that the jump rate from P^R into P^F must be much slower than the lifetime of P^F. Thus, the transition rate between a P^R substate and P^F and vice versa is entirely determined by the upward jump rate (w in Fig. 8). It can be shown, using the qualitative model for the three-electron spin state P^F, outlined above, that only mixing between T_+ and T_0, or between T_- and T_0 occurs (the singlet state is also involved, but at lower temperatures the probability of recombination into the singlet state is negligible). Therefore, upon entering the state P^F in any of the three triplet spin configurations, no effective mixing of T_+ with T_- can occur. In the kinetic model given in Fig. 8, it is easily recognized that the model of Fig. 5 can be extracted from it, if $a,b,c,d \geqslant p$ (and thus $\gg w$).

The rate equations from the kinetic scheme in Fig. 8 can be solved using the approximation that the transitions between P^R and P^F are much faster than the decay rates from P^R to the singlet ground state. (This is not exactly true, but for $T > 40$ K a reasonable approximation.) Solving the rate equations for a steady state yields the result that the ratio of T_+/T_0 populations (equal to T_-/T_0) is independent of w, and thus of the temperature. Furthermore, this ratio is not unity. The EPR signal amplitude $S = n(T_-) - n(T_0)$ is then given by:

$$S = N[c(b+p) - a(c+d+p)] \tag{3}$$

where N is a positive function of a–d; the rate constants a–d and p are referring to Fig. 8. From the experimental results, we know that the initial amplitude in the Y^- EPR transient is absorptive and emissive for Y^+.

The approximate values of the rate constants a–d in Fig. 8, can be derived from the results discussed above. The g-value difference between the spins on P^+ and I^-, with that of the spin on Q_A^-, induces rephasing of the spins in P^F, analogous to the RPM. This rephasing frequency is of the order 10^9–10^{10} s^{-1}, using experimental values for an isotropic g-value difference and the magnetic interaction between I^- and Q_A^-. Thus, the constants a–d in Fig. 8 are at least one order of magnitude larger than the rate constant for decay of P^F (p in Fig. 8). Using the Hamiltonian (Eqn. 1), it is straightforward to calculate the relative transition probabilities a–d in the absence of relaxation of $Q_A^-Fe^{2+}$ [30], yielding $b \approx 20a$ and $d \approx 6c$. By further taking $a = c \approx 10p$, an absorptive EPR Y^- signal is predicted using Eqn. 3. Using these relations, after many cycles of $P^R \leftrightarrow P^F$ during the P^R lifetime, the ratio of $T_\pm$ population over that of T_0 in P^R approaches approx. 3:1, i.e., a strong non-Boltzmann distribution. The regeneration of P^F in a triplet spin configuration from P^R has a larger probability to populate the $T_\pm$ sublevels of P^F (and subsequently of P^R) than the initial creation of P^F in a singlet spin configuration. The $P^R \leftrightarrow P^F$ recycling process thus enhances the electron spin polarization of P^R during its lifetime.

When spin-relaxation within P^F is taken into account, the recombination kinetics change with temperature, (increasing the $T_\pm$ populating rate) just as described in the first part of this discussion. Thus, the numbers for a–d are expected to change, resulting in a change of the ratio $n(T_+)/n(T_0)$ of the steady state populations in T_+ and T_0.

The quadratic dependence on temperature of the observed relaxation rate within P^R (i.e., the jump rate from P^R to P^F in our model) is unusual and suggests that a phonon-bottleneck is involved [36].

The P^R pathway for charge-separation

The $P^R \leftrightarrow P^F$ mechanism may also provide understanding of the fact that the photosynthetic system of *Rps. viridis* is able to function using an unusual energy scheme.

The lowest excited singlet state of the antenna system is higher in energy than the corresponding state of P-960 [37]. Since the RC triplet energy is certainly lower than the antenna excited singlet state energy, and possibly lower than the lowest triplet state of the antenna chromophore, it is conceivable that P^F, necessary for light-driven photosynthesis, is generated from P^R and not, as is usual, from the excited singlet state P^*.

In this respect the following intriguing observations are relevant: the sign of transitions in the ODMR spectra of *Rps. viridis* chromatophores [38] is the same as that in ODMR spectra from RC's [39]. In all other studied photosynthetic species the sign of the ODMR transitions in spectra of chromatophores or cells, containing both antennas and RC's, is opposite to the sign of these transitions in ODMR spectra of preparations containing exclusively RC's. The sign inversion in chromatophores and cells is explained by singlet–singlet energy transfer between antenna and the primary donor in the RC [40,41].

If it is assumed that the energy from the antenna system is transferred to the RC by a triplet–triplet energy-transfer mechanism, it is easily recognized that the sign of the ODMR transitions should be the same for RC's with and without antennas. The charge separation, according to the model given above would now have to occur via the $P^R \rightarrow P^F$ reaction, again yielding the $P^+Q_A^-$ charge separated state. At low temperatures, under conditions where the ODMR experiments are performed, this back reaction is very slow (less than $10^3\ s^{-1}$). It should thus be noticeable in time-resolved low-temperature optical absorption measurements.

The initial low temperatures ESP pattern of P^R in antenna containing preparations, exclusively generated via an antenna triplet state, would be different from the AEEAAE pattern observed for isolated RC's. Furthermore, it is to be expected that the generation of P^+ from the excited antenna is temperature dependent.

Appendix A. Calculation of the P^R spin-lattice relaxation rate

From the rate equations of the model schematically given in Fig. 5, it is easy to extract the secular equation in w:

$$(3\lambda - 2k_1 - k_0)w^2 + \{-4\lambda^2 + 2\lambda(3k_1 + k_0) - 2(k_1^2 + k_0k_1)\}w + \lambda^3 - \lambda^2(2k_1 + k_0) + \lambda(k_1^2 + 2k_0k_1) - k_0k_1^2 = 0 \qquad \text{(A-1)}$$

where λ is the experimentally measured decay rate constant. Substituting one of the two observed decay rate constants λ in Eqn. A-1 and using the k_0 and k_1 values at 4 K, two possible values for w are found (for the Z EPR transients a single w is found using Eqn. A-1). The solutions of λ are of the form:

$$\lambda_1 = k_0 + f_1(w, k_0, k_1)$$

$$\lambda_2 = k_1 + f_2(w, k_0, k_1)$$

For $T \rightarrow 0$ K, $f_i \rightarrow 0$ $(i = 1, 2)$. Thus, by extrapolating the observed λ's to $T \rightarrow 0$ K, one can decide which w to take, since only one of the two possible w values has the correct limiting value (k_0) for $T \rightarrow 0$ K.

From Eqn. A-1 and the above-mentioned limiting condition, we can find a value of w for any value of λ; since the dependence of λ on T is experimentally obtained, the temperature dependence of w is found (see Fig. 6).

Appendix B. The effect of relaxation on the polarization inversion of the Y transitions

We consider a T_0 populated triplet state ($p_0 = 1$, $p_1 = 0$) with different SLR rate constants w_{ij} ($i < j = \pm 1, 0$) at high magnetic field, connecting any pair of sublevels with decay constants $k_{+1} = k_{-1} = k_1$ and k_0. The ratio w_{ij}/w_{ji} is determined by the Boltzmann factor $\alpha = e^{-\Delta E/kT}$. It is assumed that $E(+1) - E(0) = E(0) - E(-1)$, so that only a single factor α is required. Solving the steady-state rate equations, we obtain:

$$\text{sign}\{n_+ - n_0\} = \text{sign}[(\alpha - 1)\{\alpha w_{+1,0}w_{0,-1} + \alpha w_{0,-1}w_{+1,-1} + \alpha^2 w_{+1,0}w_{+1,-1} + w_{+1,0}k_1\} - k_1\{(\alpha^2 + 1)w_{+1,0} + \alpha w_{0,-1} + k_1\}] \qquad \text{(B-1)}$$

Since $0 < \alpha < 1$, and all rate constants are positive, both terms on the right-handside on Eqn. B-1 are negative. Therefore $n_+ - n_0 < 0$ for any set of parameters p_0, k_0, w_{ij} at any temperature, indicating an absorptive EPR signal under all (steady-state) conditions. The observation that the absorptive Y^+ peak of P^R at $T < 20$ K converts into an emissively polarized transition at $T > 20$ K therefore cannot be caused by an relaxation process within P^R.

Acknowledgements

We thank Dr. P. Gast (University of Chicago) for useful discussions in an early stage of this work. R. Spruijt grew the bacterial cells and isolated some of the RC's. We enjoyed stimulating discussions with Dr. P.J. Hore and Mr. D.A. Hunter (Oxford), initiated by Dr. A.J. Hoff.

References

1 Dutton, P.L., Leigh, J.S. and Siebert, M. (1972) Biochem. Biophys. Res. Commun. 46, 406–413.
2 Norris, J.R. and Katz, J.J. (1978) in The Photosynthetic Bacteria (Clayton, R.K. and Sistrom, W.R., eds.), pp. 397–418, Plenum, New York.
3 Thurnauer, M.C., Katz, J.J. and Norris, J.R. (1975) Proc. Natl. Acad. Sci. USA 72, 3270–3274.
4 Schaafsma, T.J., Kleibeuker, J.F., Platenkamp, R.J. and Geerse, P. (1976) in Molecular Spectroscopy of Dense Phases, Proceedings of the 12th Congress on Molecular Spectroscopy, Strassbourg, France, 1975, pp. 491–494.
5 Hoff, A.J. (1979) Phys. Rep. 54, 75–200.
6 Hoff, A.J. (1982) Biophys. Struct. Mech. 8, 107–150.
7 Hoff, A.J. (1984) Q. Rev. Biophys. 17, 153–282.
8 Hoff, A.J. (1982) in Triplet State ODMR Spectroscopy (Clarke, R.H., ed.), pp. 367–425, Wiley, New York.
9 Rockley, M.G., Windsor, M.W., Cogdell, R.J. and Parson, W.W. (1975) Proc. Natl. Acad. Sci. USA 72, 2251–2255.
10 Schenck, C.C., Parson, W.W. Holten, D. and Windsor, M.W. (1981) Biochim. Biophys. Acta 635, 383–392.
11 Holten, D., Windsor, M.W., Parson, W.W. and Thornber, J.P. (1978) Biochim. Biophys. Acta 501, 112–127.
12 Parson, W.W. and Monger, T.G. (1976) Brookhaven Symp. Biol. 28, 195–212.
13 Rutherford, A.W., Paterson, D.R. and Mullet, J.E. (1981) Biochim. Biophys. Acta 635, 205–214.
14 Frank, H.A., McLean, M.B. and Sauer, K. (1978) Proc. Natl. Acad. Sci. USA 76, 5124–5128.
15 Swarthoff, T., Gast, P. and Hoff, A.J. (1981) FEBS Lett. 127, 83–86.
16 Van Wijk, F.G.H., Gast, P. and Schaafsma, T.J. (1985) in Antennas and Reaction Centers of Photosynthetic Bacteria (Michel-Beyerle, M.E., Ed.), p. 146, Springer, Berlin.
17 Van Wijk, F.G.H., Gast, P. and Schaafsma, T.J. (1986) Photobiochem. Photobiophys. 11, 95–100.
18 Van Wijk, F.G.H., Beijer, C.B. Gast, P. and Schaafsma, T.J. (1987) Photochem. Photobiol. 46, 1015–10119.
19 Van Wijk, F.G.H., Gast, P. and Schaafsma, T.J. (1986) FEBS Lett. 206, 238–242.
20 Hoff, A.J. and Proskuryakov, I.I. (1985) Chem. Phys. Lett. 115, 303–310.
21 Gast, P. and Hoff, A.J. (1978) FEBS Lett. 85, 183–188.
22 Windsor, M.W. and Holten, D. (1980) Phil. Trans. R. Soc. Lond. A298, 335–349.
23 Chidsey, C.E.D., Takiff, L., Goldstein, R.A. and Boxer, S.G. (1985) Proc. Natl. Acad. Sci. USA 82, 6850–6854.
24 Hoff, A.J. and Hore, P.J. (1984) Chem. Phys. Lett. 108, 104–110.
25 Shuvalov, V.A. and Parson, W.W. (1981) Biochim. Biophys. Acta 638, 50–59.
26 Woodbury, N.W., Parson, W.W., Gunner, M.R., Prince, R.C. and Dutton, P.L. (1986) Biochim. Biophys. Acta 851, 6–22.
27 Gunner, M.R., Robertson, D.E. and Dutton, P.L. (1986) J. Phys. Chem. 90, 3783–3795.
28 Wraight, C.A. (1977) Biochim. Biophys. Acta 548, 309–327.
29 Den Blanken, H.J. and Hoff, A.J. (1982) Biochim. Biophys. Acta 681, 365–374.
30 Van Wijk, F.G.H. (1987) Thesis, Wageningen Agricultural University, The Netherlands.
31 De Jager, P.A. and Van Wijk, F.G.H. (1987) Rev. Sci. Instrum. 58, 735–741.
32 Van Hoek, A. and Van Wijk, F.G.H. (1987) Appl. Opt. 26, 1164–1166.
33 McLachlan, L.A. (1977) J. Magn. Reson. 26, 223–228.
34 Levanon, H. and Vega, S. (1974) J. Chem. Phys. 61, 2265–2274.
35 Dismukes, G.C., Frank, H.A., Friesner, R. and Sauer, K. (1984) Biochim. Biophys. Acta 764, 253–271.
36 Abragam, A. and Bleaney, B. (1970) Electron Paramagnetic Resonance of Transition Ions, pp. 541–584, Clarendon Press, Oxford.
37 Holt, A.S. and Clayton, R.K. (1965) Photochem. Photobiol. 4, 329–331.
38 Van Wijk, F.G.H., Schaafsma, T.J. and Michel, H. (1984) Advances in Photosynthesis Research (Sybesma, C., ed.), Vol. 2, pp. 173–176, Martinus Nijhoff/Dr. W. Junk Publishers, Dordrecht.
39 Den Blanken, H.J., Jongenelis, A.P.J.M. and Hoff, A.J. (1983) Biochim. Biophys. Acta 725, 472–482.
40 Hoff, A.J. and De Vries, H.G. (1978) Biochim. Biophys. Acta 681, 32–40.
41 Hála, J., Searle, G.F.W., Schaafsma, T.J., Van Hoek, A., Pancoska, P., Bláha, K. and Vacek, K. (1986) Photochem. Photobiol. 44, 527–534.
42 Hore, P.J., Hunter, D.A., Van Wijk, F.G.H. and Schaafsma, T.J. (1988) Biochim. Biophys. Acta 936, 249–258.